

# Analytical Relationships Between Conflict Counts and Air-Traffic Density

Matt R. Jardin\*

NASA Ames Research Center, Moffett Field, California 94035

Semi-empirical random variable models of the expected number of air-traffic conflicts as a function of air-traffic density are derived. Model parameters are determined from analysis and simulation of real air-traffic data. These models are applied to simulated air-traffic scenarios to analyze conflict properties in various conflict resolution strategies. It is shown that under free routing conditions (approximated by great-circle routes in zero-wind conditions) the expected number of conflicts is well represented by a binomial random variable model. Using this model, it is further demonstrated how conflict resolution can cause a chain reaction, leading to an increased number of conflicts for all aircraft, and how the model can be used to predict the airspace capacity for a given conflict resolution strategy. In a separate study, it is shown that for an iterative horizontal-plane conflict resolution strategy, a random variable model with the geometric distribution closely matches empirical data. This model also predicts the aircraft density at which the airspace becomes saturated. It is shown how analysis of conflicts in the horizontal plane can be scaled and applied to the analysis of conflicts in three-dimensional airspace.

## Introduction

CURRENT en route air-traffic-control (ATC) operations are based on the use of structured jet routes. Aircraft are rarely permitted to operate along unstructured routes unless air traffic is sparse. The concept of free flight for ATC has arisen from the desire to create more efficient en route air-traffic operations.<sup>1</sup> The idea is that by allowing aircraft to determine and update their own unstructured flight routes while using automated onboard conflict detection and resolution algorithms the ATC system will be more efficient. In low air-traffic densities, as is the case with the current level of air traffic, some form of free flight is predicted to provide an efficiency benefit. At some increased level of air-traffic density, airspace complexity becomes so great that efficiency benefits can no longer be realized when aircraft fly along unstructured routes. It has been theorized that with increasing air-traffic density, resolving conflicts will cause an increased number of conflicts. Simulation studies have been conducted in prior work and have shown that such a chain reaction might become significant at roughly three times the current air-traffic density,<sup>2</sup> but physical explanations have not yet been offered.

In this paper, probabilistic models of two different types of air-traffic management systems are derived and analyzed to gain insight into the relationship between increasing air-traffic density and the expected number of conflicts between aircraft. The first is a local, or decentralized, air-traffic management system where aircraft attempt to resolve only the most immediate conflicts in a distributed manner. The second system to be examined is that of a globally optimized air-traffic management system where optimal conflict-free trajectories are determined for all aircraft on a strategic timescale. Both of these strategies have been proposed as means of achieving better efficiency in air-traffic operations in the future.

The first section of this paper examines the expected number of conflicts under both a structured routing system and under a free routing system as represented by great-circle routes. It is shown that

a binomial random variable model closely matches observations of the number of conflicts when conflict resolution is not applied. The effect of conflict resolution maneuvering on the expected number of conflicts is also examined. An analytical model is derived, and simulation results are generated to verify the model.

The second main section of this paper examines a model of global air-traffic conflict resolution as opposed to the local conflict resolution model in the first section. This second section introduces a model of the expected number of conflicts when a global, iterative approach to conflict resolution is taken. The model is examined to show how it can be used to predict maximum airspace capacity for a global air-traffic optimization approach. The present analysis is concerned only with the computational issues involved in conflict resolution and does not address other practical issues that can affect capacity, such as controller workload and communications bandwidth. These issues would need to be addressed for any particular implementation of an air-traffic management system, but this is left for future work.

## Local (Decentralized) Conflict Resolution Models

In this section, probabilistic models of local (sometimes referred to as decentralized or distributed) conflict resolution processes are derived. The first model is of the expected number of conflicts when conflict resolution is not applied. The next model is of the expected number of conflicts with conflict resolution applied. A simulation is developed, and the results of the simulation are presented.

## Modeling Conflicts Without Conflict Resolution

A study performed at the NASA Ames Research Center examined the properties of air-traffic conflicts for both structured routing and great-circle routing.<sup>2</sup> In the NASA study, winds were not modeled so that great-circle routing was assumed to represent a free routing strategy. Some difference in conflict properties would be expected for optimal wind routes as compared to great-circle routes because these routes are geometrically dissimilar, but the difference is expected to be slight and should not affect the qualitative nature of the conflict-count results in this paper. Flight plan data were taken from the Enhanced Traffic Management System (ETMS) for a 24-h period in March 2000. The Future Air Traffic Management Concepts Evaluation Tool (FACET)<sup>3</sup> was used to simulate aircraft flying either along the filed flight plans or along great-circle routes between the scheduled origin and destination airports within Class A airspace (above FL180). At each 15-s integration time step, the number of active conflicts in the airspace was recorded, as was the total number of aircraft in the airspace at that time.

Received 10 August 2004; presented as Paper 2004-6393 at the AIAA 4th Aviation Technology, Integration, and Operations Forum, Chicago, IL, 20–22 September 2004; revision received 5 November 2004; accepted for publication 7 November 2004. This material is declared a work of the U.S. Government and is not subject to copyright protection in the United States. Copies of this paper may be made for personal or internal use, on condition that the copier pay the \$10.00 per-copy fee to the Copyright Clearance Center, Inc., 222 Rosewood Drive, Danvers, MA 01923; include the code 0731-5090/05 \$10.00 in correspondence with the CCC.

\*Aerospace Engineer, MS 210-10, Code AFC, Automation Concepts Research Branch, Senior Member AIAA.

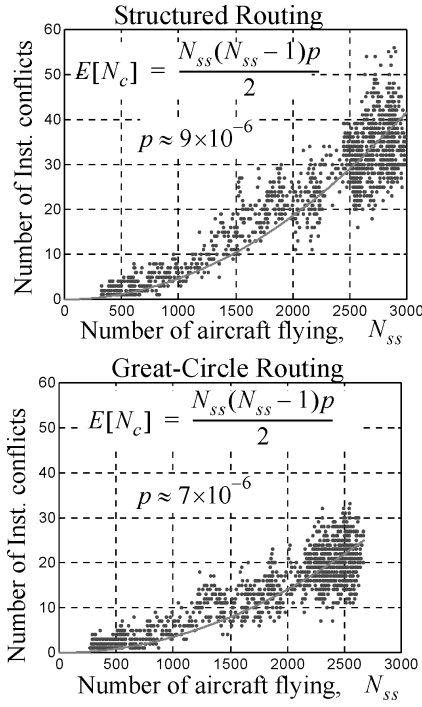


Fig. 1 Conflict counts for structured and great-circle routes.

These conflict data can be used to evaluate the aircraft density of the airspace environment. A high number of conflicts and a steep rate of growth of conflicts would suggest that the airspace was nearing saturation. Conversely, a low number of conflicts and a shallow growth rate would suggest that the airspace still had plenty of extra maneuvering volume remaining.

The plot of the number of instantaneous conflicts vs the number of aircraft flying shows that for both structured routing and great-circle routing the number of conflicts is relatively low, and the growth rate is also low (Fig. 1). Without assuming any prior knowledge of aircraft paths, it is equally likely that one aircraft will be in conflict with any other aircraft. This suggests that the instantaneous number of conflicts  $X$  for any aircraft can be modeled as a binomial random variable such that the probability mass function is given by

$$P(X = x) = \binom{n}{x} p^x (1 - p)^{n-x} \quad \begin{cases} 0 \leq p \leq 1 \\ x = 0, 1, \dots, n \end{cases} \quad (1)$$

where  $n \equiv (N_{ss} - 1)$ ,  $N_{ss}$  is the steady-state number of aircraft flying (a measure of aircraft density for a given airspace area),  $p$  is the probability that any one aircraft will have a conflict with any one other aircraft at a given instant, and

$$\binom{n}{x} \Rightarrow n \text{ choose } x \Rightarrow \frac{n!}{x!(n-x)!} \quad (2)$$

With this model, the expected number of instantaneous conflicts for a single aircraft in a field of  $N_{ss}$  aircraft is given by

$$E[X_N] = (N_{ss} - 1)p \quad (3)$$

and the expected sum total number of instantaneous conflicts (divided in half so that conflicts are not counted twice) is given by

$$C_{INST} \equiv \sum_{i=1}^{N_{ss}} \frac{E[X_i]}{2} = \frac{N_{ss}(N_{ss} - 1)p}{2} \quad (4)$$

By choosing the aircraft-to-aircraft conflict probability  $p$  to fit the data in a least-square error sense, the probabilities and expected values can be estimated for structured or great-circle routing. A table of results is presented based on the data shown in Fig. 1 (Table 1).

Table 1 Conflict statistics from binomial random variable model

| Statistic                            | Description   | Flight plan        | Great circle       |
|--------------------------------------|---|--------------------|--------------------|
| $p$                                  | Probability of aircraft $i$ conflicting with any other aircraft $j$ at a given instant in time                | $9 \times 10^{-6}$ | $7 \times 10^{-6}$ |
| $E[X_{3000}]$                        | Expected number of conflicts per aircraft in class A airspace with 3000 aircraft at any given instant in time | 0.027              | 0.021              |
| $\sum_{i=1}^{3000} \frac{E[X_i]}{2}$ | Expected sum total number of conflicts in class A airspace with 3000 aircraft at any given instant in time    | 40.5               | 31.5               |

These probabilities and expected numbers of conflicts are relatively low. In a field of 3000 aircraft in class A airspace above the continental United States, only about 2% of the aircraft would be expected to be involved in a conflict alert at any instant in time if no air-traffic-control action were taken. Conflict probabilities are lower for great-circle routing than for flight plan routing presumably because aircraft are able to utilize a greater amount of airspace.

The model in Eq. (4) can be extended to estimate the total number of expected conflicts  $C_{NR}$  for all aircraft in a given airspace area over a given interval of time when conflict resolution is not applied. In this case,  $p$  represents the probability that an aircraft  $i$  would experience a conflict alert with any other aircraft  $j$  during the analysis interval of time  $T$ . This probability can be decomposed into parts that are dependent upon airspace parameters and those that are not.

Considering an airspace of area  $A$ , which is divided into  $N_{\Delta A}$  elements of area  $\Delta A$ , the probability that any two aircraft  $i$  and aircraft  $j$  will occupy the same area element  $\Delta A$  at the same time is given by

$$\Delta p = (\Delta A/A)^2 \quad (5)$$

Summing over all area elements leads to

$$p = N_{\Delta A} (\Delta A/A)^2 = \Delta A/A \quad (6)$$

The area of an element can be written in terms of the average area swept out by an aircraft as follows:

$$\Delta A = p_t (D_{sep} \cdot V \cdot T) \quad (7)$$

where  $D_{sep}$  is the minimum separation distance between aircraft,  $V$  is the average aircraft speed,  $T$  is the time interval over which conflicts are counted, and  $p_t$  is a parameter that can be adjusted to match empirical data. The  $p_t$  parameter enables adjustments to be made for any differences between the proposed probability model and real data. For example, if aircraft are concentrated in clusters rather than uniformly distributed throughout the airspace, then the assumptions that led to Eq. (4) would no longer be valid. The  $p_t$  parameter provides a mechanism for adjusting the model to fit real-world data in these cases. Combining Eqs. (6) and (7) leads to the following expression for the probability of conflict between any two aircraft:

$$p = p_t [(D_{sep} \cdot V \cdot T)/A] \quad (8)$$

Writing  $p$  in this form separates out the dependency on airspace parameters so that the effects of changes in these parameters can more easily be discerned.

Equation (4) can be written in terms of airspace density  $\rho_{AC}$  by noting that

$$N_{ss} = \rho_{AC} \cdot A \quad (9)$$

Substituting Eqs. (8) and (9) into Eq. (4) leads to the following expression for  $C_{NR}$ , the total number of conflicts if no resolution is applied:

$$C_{NR} = p_t [(D_{sep} \cdot V \cdot T \cdot A)/2] \rho_{AC} (\rho_{AC} - 1/A) \quad (10)$$

### Modeling Conflicts with Conflict Resolution: Conflict Chain Reactions

A conflict alert is defined as a condition in which two aircraft are predicted to be closer together than a specified minimum separation distance within a specified look-ahead distance (or time). Resolving aircraft conflicts using decentralized techniques can result in a chain reaction, which increases the number of conflict alerts. If the increase in the number of conflicts is pronounced, the conflict resolution algorithms leading to the increase might be unstable. A study of this phenomenon was presented in Ref. 4. Note that it is the uncertainty in predicting conflict alerts that ultimately causes conflict chain reactions. The uncertainty can either be from imperfect intent information, or errors in trajectory prediction. Intent uncertainty arises from the complexity of high aircraft density because one cannot determine a priori how each conflict situation will be resolved in a decentralized system. Though not explored in detail in this paper, the techniques developed here might also be used to explore the effects of trajectory prediction uncertainty by treating conflict alerts as probabilistic rather than deterministic. One can choose to explore the effects of different thresholds at which a conflict alert is considered to be active.

The increase in conflicts as a result of conflict resolution was quantified in Ref. 4 by the “domino effect parameter (DEP),” defined as

$$\text{DEP} \equiv (C_{\text{WR}}/C_{\text{NR}} - 1) \quad (11)$$

where  $C_{\text{NR}}$  is the number of conflict alerts with no conflict resolution and  $C_{\text{WR}}$  is the number of conflict alerts with conflict resolution applied.

A physical model is proposed in this section to explain conflict resolution chain reactions. The system considered is similar to that in Ref. 4. Aircraft are randomly generated at the same altitude in a 100 n mile radius airspace and are flying at the same ground speed. After conflicts are resolved, the aircraft are directed back to their originally planned exit point. Details of the conflict resolution are given later in the simulation results section of this paper.

The hypothesis is that for a given aircraft density in such a system the rate of occurrence of conflict alerts (number of conflict alerts per unit time or distance) is constant whether or not aircraft perform conflict resolution maneuvers. This hypothesis is derived from the idea that there should be no preferred direction in such a system. It should be equally likely for any aircraft flying in any direction to experience a conflict. Just because an aircraft maneuvers does not change this fact. What does change is the total distance of flight in the test airspace and the amount of airspace searched for conflicts. If the rate of conflicts is constant, but the total distance flown and searched for conflicts by all aircraft increases as a result of conflict resolution maneuvering, then one would expect the overall number of conflicts to increase. As aircraft density increases and more conflict resolution maneuvers are required, the additional distance flown would also increase.

The expected number of conflicts  $C_i$  for aircraft  $i$  is expressed as

$$C_i = \bar{L} \cdot r_c \quad (12)$$

where  $\bar{L}$  is the average path distance and  $r_c$  is the average rate of conflicts per unit distance.

The path distance is now modeled to increase in proportion to the number of conflicts so that Eq. (12) becomes

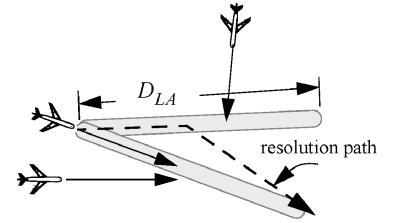
$$C_i = (L + k \cdot C_i) r_c \quad (13)$$

where  $L$  is the average nominal path distance of the aircraft in the simulation airspace without conflict resolution applied and  $k$  is a constant model parameter, which includes both the average amount of extra path distance flown as a result of conflict resolution and the effective extra path distance searched for conflicts per conflict resolution. As shown in Fig. 2, the effective amount of airspace searched for conflicts depends on the conflict look-ahead distance and the length of the resolution portion of the trajectory.

Solving Eq. (13) for  $C_i$  leads to

$$C_i = (L \cdot r_c) / (1 - k \cdot r_c) \quad (14)$$

**Fig. 2 Conflict resolution maneuvers cause additional airspace to be searched for conflicts.**



Summing over  $N_{\text{AC}}$  aircraft, where  $N_{\text{AC}}$  is the total number of aircraft flying through the airspace (not the same as  $N_{\text{ss}}$ ), leads to the following expression for the total number of conflicts with conflict resolution applied:

$$C_{\text{WR}} = \frac{N_{\text{AC}} \cdot L \cdot r_c}{1 - k \cdot r_c} \quad (15)$$

The total number of conflict alerts without conflict resolution applied was given in Eq. (10). By the original hypothesis, the conflict rate should be the same for both the with-resolution and no-resolution cases. Using the no-resolution expression, the conflict rate can be written as the total number of no-resolution conflict alerts divided by the total path distance:

$$r_c = C_{\text{NR}} / (N_{\text{AC}} \cdot L) \quad (16)$$

To maintain a given average airspace density over a given area and time, the number of aircraft must be

$$N_{\text{AC}} = \rho_{\text{AC}} \cdot A \cdot T \cdot (V/L) \quad (17)$$

Substituting Eqs. (10) and (15–17) into Eq. (11) leads to the following relation for the domino effect parameter:

$$\text{DEP} = \frac{(\rho_{\text{AC}} - 1/A)}{\rho_{\text{max}} - (\rho_{\text{AC}} - 1/A)} \quad (18)$$

where  $\rho_{\text{max}}$  is defined as

$$\rho_{\text{max}} \equiv 2 / (k \cdot p_t \cdot D_{\text{sep}}) \quad (19)$$

This parameter can either be chosen for analysis purposes, or determined empirically by adjusting its value until Eq. (18) best fits empirical data.

For values of  $\rho_{\text{AC}}$  much greater than  $1/A$ , an approximate version of Eq. (18) is given by

$$\text{DEP} \approx \rho_{\text{AC}} / (\rho_{\text{max}} - \rho_{\text{AC}}) \quad (20)$$

Note that  $\rho_{\text{max}}$  can be considered as a measure of the airspace capacity for the given conflict resolution scheme. The model of either Eq. (18) or (20) predicts that the chain reaction of conflicts will become infinite when  $\rho_{\text{AC}}$  approaches  $\rho_{\text{max}}$ , which makes intuitive sense because there is a finite amount of airspace. This leads to a practical and realistic means of computing the airspace capacity for a free-flight type of system with local conflict resolution.

### Local Conflict Resolution Simulation Results

Monte Carlo simulations of randomly generated traffic have been run to generate data to validate the conflict model derived in this paper. Three different cases have been run for different values of separation distance  $D_{\text{sep}}$  and conflict look-ahead distance  $D_{\text{LA}}$  to examine their effects upon conflict resolution. Each case was run with no resolution and with resolution at multiple values of  $N_{\text{ss}}$ , and multiple simulations were run for each value of  $N_{\text{ss}}$  in order to achieve some statistical variability. The pseudo-random-number generator from MATLAB<sup>®</sup> was used to generate repeatable random cases so that the same traffic was run through both the no-resolution and with-resolution cases. The cases and values of  $N_{\text{ss}}$  used are given in Table 2. The remaining parameters were common to all three cases and are given in Table 3.

The details of how conflict resolution is performed and how conflicts are counted are as follows:

**Table 2** Definitions of simulation cases

| Case | $D_{sep}$ ,<br>n miles | $D_{LA}$ ,<br>n miles | $\{N_{ss}\} \times \#$ of sims  |
|------|------------------------|-----------------------|---|
| 1    | 5                      | 66.7                  | $\{5, 10, \dots, 35\} \times 15$<br>$\{40, 45, 50, 60, 80\} \times 3$ |
| 2    | 2.5                    | 66.7                  | $\{5, 10, \dots, 50, 60, 80, 85\} \times 3$                           |
| 3    | 5                      | 16.7                  | $\{5, 10, \dots, 50, 60, 80, 85\} \times 3$                           |

**Table 3** Simulation parameters

| Parameter  | Value(s)                  | Notes  |
|------------|---------------------------|--|
| $R$        | 100 n miles               | Circular simulation area of radius $R$   |
| $\bar{V}$  | 500 kn                    | All aircraft traveling at the same speed $\bar{V}$   |
| $\bar{L}$  | $(4/\pi)R$                | Average path distance for uniformly random generated traffic across a circular area of radius $R$  |
| $T$        | 65.3 min                  | Simulation time duration. Note that simulation is also initialized for a duration of $\bar{L}/\bar{V}$ prior to starting data collection in order to populate the airspace |
| $\Delta T$ | 2 s                       | Simulation time-step size  |
| $r_{AC}$   | $N_{ss}(\bar{V}/\bar{L})$ | Rate of introduction of aircraft into simulation airspace to achieve $N_{ss}$ steady-state aircraft  |

1) Conflict resolution maneuvers are computed according to the geometric conflict resolution algorithm in Ref. 5. Conflict resolution is noncooperative such that only one aircraft involved in each conflict will maneuver. Of the multiple potential resolution solutions, the one that produces the greatest relative velocity is chosen in an effort to minimize the time to the turn-back point, where the aircraft can turn back to its original destination. The aircraft with the longest distance to go is the one to make the resolution maneuver.

2) Aircraft that are generated with very short nominal paths are discarded, with new random paths being generated until nominal path distances are greater than 10% of the circle radius.

3) Aircraft that start with pop-up conflicts with line-of-sight distance less than  $D_{sep}$  are allowed to continue, with a conflict being counted for the pop-up conflict.

4) At each time step, the turn-back path to the destination point is checked. Once it is clear, the aircraft turns back.

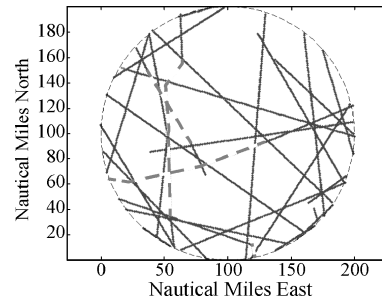
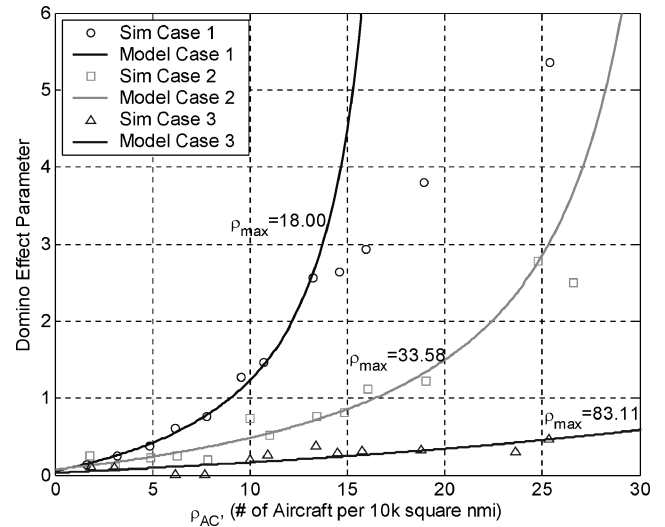
5) If the turn-back path results in a conflict with a different aircraft than the one that caused the original conflict, then the turn-back path is taken, but the aircraft resolves the new turn-back conflict.

6) Multiple conflicts between any specific aircraft pair are only counted as one conflict. This might miss some repeat conflicts that can occur after multiple resolution maneuvers, but eliminates the overcounting of chattering conflicts. A chattering conflict is a situation in which a resolution maneuver immediately results in a conflict with a different aircraft. When this second conflict is resolved, the resolution causes the original conflict to recur, and this results in a repeating, or chattering, conflict cycle.

7) Conflict look-ahead is extended outside the circle so that conflicts which are projected to occur outside the circle are counted, and resolution maneuvers made. However, the rate of conflicts outside the circle will diminish with distance away from the circle because the aircraft density falls off quickly. Ideally, look-ahead distance should be small compared with the circle radius.

8) Aircraft that maneuver to avoid conflicts and pass outside the circle are dropped from the simulation at the point where they exit the circle. This is a mechanism by which the airspace capacity limit manifests itself as aircraft are bounced outside of the simulation airspace.

A plot of the recorded trajectories is shown (Fig. 3) for a 65-min simulation with a minimum separation distance of 5 n miles and an average of five aircraft within the 100 n mile circle in steady state. The conflict resolution segments are highlighted in dashed red lines. This particular simulation had two aircraft that experienced multiple chain-reaction conflicts.

**Fig. 3** Recorded trajectories for a 65-min simulation with  $N_{ss} = 5$  and  $D_{sep} = 5$  n miles.**Fig. 4** Simulation data and models of conflict resolution chain reactions.

The results of the Monte Carlo simulation runs for the three different cases have been plotted together for comparison with one another (Fig. 4). The nominal case (sim. case 1), with  $D_{sep} = 5$  n miles and  $D_{LA} = 66.7$  n miles, shows a clear trend along the curve predicted by Eq. (18) until the aircraft density exceeds 14 aircraft per  $10^4$  square n miles. As predicted by the model, an aircraft density is reached at which the airspace begins to become saturated. Because the simulation is of a finite airspace area, aircraft begin to be bounced outside of the airspace boundary as a result of conflicts as the airspace density limit is approached. Once these aircraft leave the simulation airspace, their conflicts are no longer counted, and this is why the empirical curve departs from the theoretical curve. The data points prior to the density limit being reached are used to determine the value of  $\rho_{max}$ , which provide a best fit of Eq. (18) to the empirical data in a least-square error sense.

Reducing the separation distance by a factor of two (sim. case 2), from 5 to 2.5 n miles increased the value of  $\rho_{max}$  by a factor of two. Again, the departure of the simulation results from the model occurred when the aircraft density exceeded a critical threshold. For the parameters used in the simulation, the parameter  $k$  is dominated by the conflict look-ahead distance so that changes in the look-ahead distance should cause inversely proportional changes in  $\rho_{max}$ . A factor of four reduction in the conflict look-ahead distance from 8 min (equivalently 66.7 n miles at  $V = 500$  kn) to 2 min (16.7 n miles) did result in approximately a factor of four increase in  $\rho_{max}$  as shown in Fig. 4 (sim. case 3).

#### Discussion of Local Conflict Resolution Results

The derived conflict model clearly shows that reductions in either separation distance or look-ahead distance will increase the airspace capacity by a proportional amount. This suggests a method for considering global airspace efficiency when deciding how to perform local conflict resolution.

Prior research considered the efficiency of conflict resolution maneuvering with trajectory prediction uncertainty.<sup>6</sup> It was shown that

the expected extra distance flown could be minimized by resolving conflicts at an optimum conflict time horizon. As airspace density increases, the cascading effect of resolving conflicts too early (by having too large of a look-ahead time) incurs a large global penalty in efficiency. When global efficiency is considered, the optimum time horizon for performing conflict resolution will generally be different than if only individual aircraft efficiency were considered. This would be an interesting topic for future research.

### Global (Centralized) Conflict Resolution Model: Sequential Conflict Resolution

The preceding section of this paper described models of the number of conflicts that might arise in a decentralized type of air-traffic management system. Global (sometimes referred to as centralized) conflict resolution strategies have also been proposed for air-traffic management. Global conflict resolution differs from local conflict resolution in that all aircraft trajectories and conflicts are considered and resolved simultaneously. The potential benefit of global conflict resolution is that one might be able to achieve the globally optimum (e.g., minimum time, minimum path deviation, or minimum fuel) solution. In airspace with relatively few aircraft, either local or global strategies tend to produce similar results, but as airspace density increases one would expect the global strategy to produce a more organized and efficient result by utilizing global situational knowledge of the airspace. In this section, analytical models of a global conflict resolution strategy are derived.

Many different types of global conflict resolution systems might be envisioned. In this section, a model is derived for a particular type of global conflict resolution based on optimal wind routes with sequential resolution of conflicts. This might be considered as a representative system that produces the global optimum solution with perturbations to individual aircraft introduced only as necessary to resolve conflicts. The resulting conflict-free solutions for this system have been shown to be very close to the theoretical global optimum solutions.<sup>7</sup> The conflict model is derived, followed by the presentation of simulation results.

#### Sequential Conflict Resolution Model

Sequential conflict resolution means that a conflict-free trajectory is determined for each aircraft sequentially, while holding previously planned trajectories fixed. In this paper, an optimal wind routing algorithm called neighboring optimal wind routing (NOWR) is used to generate trajectories to demonstrate the sequential procedure,<sup>7-9</sup> but other route computation algorithms might also be used.

A high-level flowchart for the sequential conflict resolution algorithm is illustrated in Fig. 5. The algorithm places all scheduled aircraft into an ordered list called the Active Aircraft List (AAL), which includes all in-flight aircraft and aircraft scheduled to depart within a specified look-ahead time window. The optimal horizontal route for the first aircraft on the AAL is computed and checked for

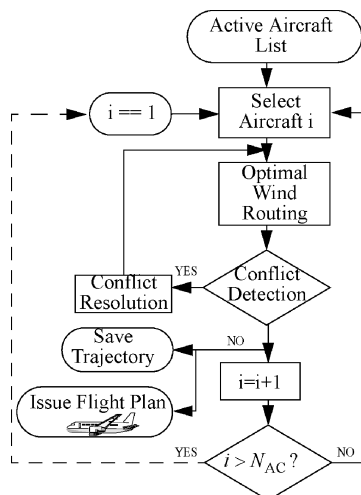


Fig. 5 Sequential optimization flowchart.

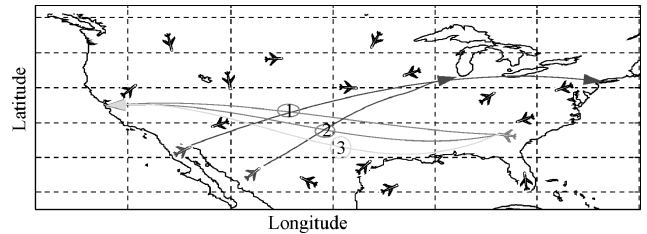


Fig. 6 Conflict resolution iterations.

conflicts. There will be no conflicts with other aircraft for the first aircraft in the AAL, but conflicts with regions of bad weather or with special-use airspace can occur. If any conflicts are found, the trajectory is iteratively modified until a conflict-free trajectory results. The algorithm proceeds through all aircraft on the AAL until all have optimal conflict-free trajectories. At this point, the trajectories can be issued to the aircraft as flight plan clearances, and the optimization procedure can be restarted as often as required.

The hypothesis is that for a sequential conflict-resolution strategy, it is equally likely at each iteration that another conflict might be encountered (Fig. 6). This can be described as a memory-less property and suggests the use of the geometric random variable (GRV) for the conflict iteration model because the GRV is the only discrete random variable with the memory-less property.

If  $R_i$  is modeled as a GRV representing the number of iterations required to resolve all conflicts for the  $i$ th aircraft, where each resolution iteration is considered to be an independent Bernoulli trial with probability  $P_i$  of being conflict free, then the probability mass function for  $R_i$  is given by

$$p_{ik} = P_i(1 - P_i)^{(k-1)} \quad \begin{cases} i = 1, 2, \dots, N \\ k = 1, 2, \dots \end{cases} \quad (21)$$

where  $p_{ik}$  is the probability of resolving a conflict in  $k$  iterations for the  $i$ th aircraft. Typical values of  $P_i$  are close to unity so that the probability of finding a conflict-free solution during the first iteration is high and the probability that a conflict-free trajectory will not be found until a later iteration decreases rapidly.

The expected value of the GRV,  $R_i$ , is

$$E[R_i] = 1/P_i \quad (22)$$

As an extension to the standard GRV model,  $P_i$  is modeled as a function of the aircraft number. The reason for doing so is that the probability that a particular trajectory will be conflict free decreases as the number of aircraft increases. The first aircraft will have a conflict-free trajectory with probability 1, whereas later aircraft will have increasing conflict probabilities. A linear form for  $P_i$  is chosen as

$$P_i = (C_0 + 1)/C_1 - (1/C_1)i \quad (23)$$

where  $C_0$  and  $C_1$  are parameters that are to be determined to best fit observed data. The form for the coefficients of  $P_i$  was chosen to simplify the final results. The linear functional form was chosen because it is simple and leads to a good fit to empirical data. Other functional forms such as higher-order polynomials or exponential functions might also be used. The choice of functional form for  $P_i$  primarily affects model properties as the number of aircraft increases toward a limiting upper value.

Substituting Eq. (23) into Eq. (22) leads to

$$E[R_i] = C_1/[(C_0 + 1) - i] \quad (24)$$

To generate data to curve fit Eq. (24), one would have to perform multiple simulations or experiments to generate many data points at each value of  $i$  so that the expected number of resolution iterations could be determined to some degree of statistical significance. A curve fit of these expected values as a function of  $i$  could then be used to determine  $C_0$  and  $C_1$  in a least-square error sense.

A better approach is to derive an expression for the sum of Eq. (24) over all aircraft. By doing so, only one simulation needs to be run

while maintaining a running total of the number of conflict iterations. Each element of the sum is an independent measurement so that many independent measurements contribute to the sum as a function of the number of aircraft. A curve fit of the summation function can then be used to obtain values for  $C_0$  and  $C_1$ .

The summation of Eq. (24) leads to the following analytical expression:

$$Y_N \equiv \sum_{i=1}^N E[R_i] = \sum_{i=1}^N \frac{C_1}{(1+C_0)-i} = C_1 \left[ \Psi(C_0) - \Psi(C_0 - N) - \frac{N}{C_0(C_0 - N)} \right] \quad (25)$$

where  $\Psi(x)$  is the digamma function, defined as

$$\Psi(x) \equiv \frac{d}{dx} \ln[\Gamma(x)] \quad (26)$$

and the gamma function  $\Gamma(x)$  is defined as

$$\Gamma(x) \equiv \int_0^\infty t^{(x-1)} e^{-t} dt \quad (27)$$

Although Eq. (25) is compact, it would be inconvenient to leave the expression in this form because the digamma function is not commonly used. In the region of interest for this problem, the digamma function is asymptotically close to the natural logarithm  $\ln(x)$ . This leads to the following approximate form of Eq. (25):

$$Y_N \approx C_1 \ln\left(\frac{C_0}{C_0 - N}\right) - \frac{C_1 N}{C_0(C_0 - N)} \quad (28)$$

The second term in Eq. (28) turns out to be negligible for the types of problems being analyzed so that the total number of conflicts for  $N$  aircraft is well approximated by

$$Y_N \approx C_1 \ln[C_0/(C_0 - N)] \quad (29)$$

By examining Eq. (23), one can determine some properties of the conflict-iteration model parameters. The first aircraft will only require one iteration (ignoring special-use airspace and weather cells for the moment), with probability 1, leading to the following relation:

$$P_1 = (C_0 + 1)/C_1 - 1/C_1 = 1 \quad (30)$$

and so one would expect

$$C_0 \approx C_1 \quad (31)$$

When curve fitting empirical data, the fits obtained using two parameters are much better than single-parameter curve fits because the data are not completely randomly distributed; for this reason, both parameters are retained. However, this analysis suggests that one might expect  $C_0$  and  $C_1$  to be numerically close.

Because aircraft typically cruise at near-constant altitude, a reasonable assumption is that the total number of conflicts across all flight levels is given by

$$Y_{N|3D} = N_{FL} \cdot Y_{N|2D} \quad (32)$$

where  $N_{FL}$  is the effective number of flight levels under consideration. Although conflicts often do arise between aircraft that are climbing or descending through en route airspace, the modeling assumption in Eq. (32) is still expected to produce a reasonable estimate of the three-dimensional capacity. One can reason that as aircraft climb and descend through different flight levels, in order for the total number of aircraft to be conserved, the average number of aircraft per flight level should remain constant. Although only horizontal conflict resolution maneuvers are discussed in this paper, the model is general enough that one might use it to analyze results with a wider variety of conflict resolution algorithms being applied.

For instance, if one allowed speed change or altitude change resolution maneuvers, the numbers obtained for the model parameters  $C_0$  and  $C_1$  might change, but the model would still be valid. This illuminates some of the utility of the conflict iteration model by showing how it can be used to analyze and compare different conflict resolution algorithms. Such comparison studies would make for interesting topics of future research.

The total number of aircraft  $N_{3D}$  is given by

$$N_{3D} = N_{FL} \cdot N_{2D} \quad (33)$$

Under this assumption, the form of Eq. (29) is the same for the three-dimensional problem as for the two-dimensional problem with the constants being related in the following way:

$$C_{0|3D} \equiv N_{FL} \cdot C_{0|2D} \quad (34)$$

$$C_{1|3D} \equiv N_{FL} \cdot C_{1|2D} \quad (35)$$

This assumption reduces the effort required to obtain results that apply to the full three-dimensional problem. In the common flight altitudes of class A airspace (FL180 through FL390), there are 17 distinct flight levels at which a total of up to 5000 aircraft can be found at any instant in time. Instead of running simulations of 5000 or more aircraft to determine the model parameters of Eq. (29), one can run much simpler two-dimensional simulations of about 300 aircraft (5000/17) at constant altitude. The values of  $C_0$  and  $C_1$  can be determined by curve fitting the simulation data, and then Eqs. (34) and (35) can be used to determine the equivalent values for the full class A problem. The estimate of three-dimensional capacity obtained in this way serves as an upper limit to the number of aircraft that might be accommodated if aircraft were packed into all flight levels without consideration given to flight efficiency. In current operations, aircraft are not uniformly distributed over all flight levels, but instead are concentrated near flight levels 330 through 390 where flight is most efficient. To obtain a more realistic three-dimensional capacity number, one might analyze current traffic patterns to obtain the relative distribution of traffic over all flight levels to obtain an effective number of flight levels  $N_{FL}$ , which could then be used in Eqs. (32–35).

### Sequential Conflict Resolution Simulation Results

A simulation was run to validate the derived conflict iteration model of Eq. (29). The data for the simulation were taken from the ETMS data feed for all aircraft in the continental U.S. domain at flight levels 330 and 350 on 10 August 2001. The origin, destination, and scheduled departure times were extracted from the data to generate a histogram of the number of flights during each hour along each city-pair route that appeared in the ETMS data. For the simulation, schedule data were generated randomly based on the ETMS distribution. To increase the number of flights in a realistic manner, 1.5 times the amount of actual traffic was generated in this way and used to drive the simulation according to the algorithm in Fig. 5.

For the particular simulation run shown in Fig. 7, aircraft included in the active aircraft list were those currently in the air, and those scheduled to depart within 30 min of the simulation start time. The plot shows the results of a single run through the active aircraft list. The wind data used for the simulation were from the Rapid Update Cycle, Version 2 (RUC2)<sup>10</sup> from 2100 UTC, 2-h forecast

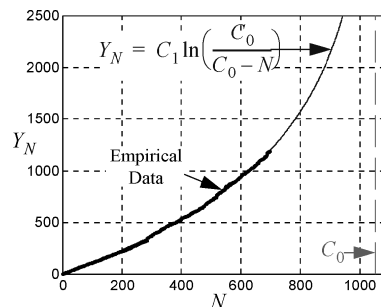


Fig. 7 Sequential conflict resolution model.

for the 225 mb pressure level. Note that 225 mb corresponds to approximately 36,000 ft.

The NOWR algorithm with iterative conflict resolution was used for route optimization. The conflict look-ahead time was set at 6.5 h, and aircraft were considered to be in conflict when their relative distance fell below 10 n miles. Optimal wind routes were generated and checked for conflicts with previously planned aircraft trajectories. If a conflict was detected, the route was perturbed slightly and checked again until a conflict-free route was found. The total number of conflict resolution iterations  $Y_N$ , as a function of the number of aircraft  $N$ , was recorded.

The shape of the  $Y_N$  vs  $N$  curve from the model matches observations well. In this particular case, for the type of perturbation conflict resolution being used the model predicts a maximum capacity of just over 1000 aircraft for a single flight level. This means that if this optimization and conflict resolution algorithm were in use, about 1000 aircraft could be accommodated before conflict-free routes could no longer be found. Note that the minimum separation distance in this example was 10 n miles, which is twice the current-day limit of 5 n miles. Also note that the route optimization algorithm being used generally does not search for conflict-free paths that weave through traffic. Other optimization algorithms might be able to effectively use more airspace to increase the upper traffic bound. By comparison, the result of this example is between two and three times the maximum number of aircraft found at a single flight level at the peak time in today's constrained air-traffic system (about 450). Simulations of other conflict resolution methods could be performed on the same data set in order to compare their performance with one another.

### Conclusions

Several semi-empirical models of aircraft conflicts have been presented in this paper. The expected number of conflicts for a given number of aircraft was shown to be well modeled as a binomial random variable. This model was extended to show how different conflict resolution strategies might lead to a conflict chain reaction and an increase in the total number of conflicts. The derived model predicts an upper limit on the number of aircraft that can operate within a given airspace. Some discussion was presented regarding how such a conflict model might be used to adjust conflict look-ahead times for distributed conflict resolution such that the total amount of extra flight distance as a result of conflict resolution is minimized over all aircraft.

For a sequential conflict resolution strategy, which is a type of global conflict resolution strategy, a semi-empirical model was developed to compute the expected number of conflict resolution iterations for a given number of aircraft. It was then shown how this model could be used to predict the capacity of a given airspace when using a particular sequential conflict resolution algorithm.

### Acknowledgments

The author thanks Karl Bilimoria and Jimmy Krozel for providing information and data from their prior work on conflict resolution modeling. The author also thanks George Meyer and Larry Meyn for their thoughtful reviews of this material and for their suggestions, which have improved the final paper.

### References

- <sup>1</sup>"Free Flight Implementation," RTCA, Inc., Final Report RTCA Task Force 3, Washington, DC, Oct. 1995.
- <sup>2</sup>Bilimoria, K. D., and Lee, H. Q., "Properties of Air Traffic Conflicts for Free and Structured Routing," AIAA Paper 2001-4051, Aug. 2001.
- <sup>3</sup>Bilimoria, K., Sridhar, B., Chatterji, G., Sheth, K., and Grabbe, S., "FACET: Future ATM Concepts Evaluation Tool," *Air Traffic Control Quarterly*, Vol. 9, No. 1, 2001, pp. 1–20.
- <sup>4</sup>Krozel, J., Peters, M., Bilimoria, K., Lee, C., and Mitchell, J. S. B., "System Performance Characteristics of Centralized and Decentralized Air Traffic Separation Strategies," *Air Traffic Control Quarterly*, Vol. 9, No. 4, 2001, pp. 311–332.
- <sup>5</sup>Bilimoria, K., "A Geometric Optimization Approach to Aircraft Conflict Resolution," AIAA Paper 2000-4265, Aug. 2000.
- <sup>6</sup>Erzberger, H., Paielli, R., Isaacson, D. R., and Eshew, M. M., "Conflict Detection and Resolution in the Presence of Prediction Error," 1st USA/Europe Air Traffic Management R&D Seminar, Eurocontrol and the Federal Aviation Administration, June 1997.
- <sup>7</sup>Jardin, M. R., "Toward Real-Time En Route Air Traffic Control Optimization," Ph.D. Dissertation, Dept. of Aeronautics and Astronautics, Stanford Univ., Palo Alto, CA, April 2003.
- <sup>8</sup>Jardin, M. R., and Bryson, A. E., Jr., "Neighboring Optimal Aircraft Guidance in Winds," *Journal of Guidance, Control, and Dynamics*, Vol. 24, No. 4, 2001, pp. 710–715.
- <sup>9</sup>Jardin, M. R., "Neighboring Optimal Aircraft Guidance in a General Wind Environment," U.S. Patent 6,600,991, 29 July 2003.
- <sup>10</sup>Benjamin, S. G., Brown, J. M., Brundage, K. J., Schwartz, B. E., Smirnova, T. G., Smith, T. L., and Morone, L. L., RUC-2—The Rapid Update Cycle Version 2, *NWS Technical Procedure Bulletin*, No. 448, National Weather Service, Office of Meteorology, Silver Spring, MD, 1998.